

1 **Extended Synaptotagmin is a presynaptic ER Ca<sup>2+</sup> sensor that**  
2 **promotes neurotransmission and synaptic growth in *Drosophila***

3

4 Koto Kikuma<sup>1,2</sup>, Daniel Kim<sup>1</sup>, David Sutter<sup>1</sup>, Xiling Li<sup>1,2</sup>, and Dion K. Dickman<sup>1,\*</sup>

5

6 <sup>1</sup>Department of Neurobiology, University of Southern California, Los Angeles, CA90089, USA

7 <sup>2</sup>USC Neuroscience Graduate Program

8

9

10

11

12

13

14

15

16

17

18

19

20

21

22

23

24

25

26

27 Running title: Synaptic functions of Esyt

28

29 Keywords: *Drosophila*, neuromuscular junction, endoplasmic reticulum, synapse

30

31

32 \*Correspondence:

33 Dion Dickman

34 Department of Neurobiology, 3641 Watt Way, HNB 309, Los Angeles, CA 90089

35 (213) 740-7533

36 [dickman@usc.edu](mailto:dickman@usc.edu)

37

38

39

40

41

42

43

44

45

46

47

48

49

50

51

52 **ABSTRACT**

53 The endoplasmic reticulum (ER) is an extensive presynaptic organelle, exerting important  
54 influences at synapses by responding to  $\text{Ca}^{2+}$  and modulating transmission, growth, lipid  
55 metabolism, and membrane trafficking. Despite intriguing evidence for these crucial functions,  
56 how presynaptic ER influences synaptic physiology remains enigmatic. To gain insight into this  
57 question, we have generated and characterized mutations in the single *Extended*  
58 *Synaptotagmin (Esy1)* ortholog in *Drosophila*. *Esy1*s are evolutionarily conserved ER proteins  
59 with  $\text{Ca}^{2+}$  sensing domains that have recently been shown to orchestrate membrane tethering  
60 and lipid exchange between the ER and plasma membrane. We first demonstrate that *Esy1*  
61 localizes to an extensive ER structure that invades presynaptic terminals at the neuromuscular  
62 junction. Next, we show that synaptic growth, structure, function, and plasticity are surprisingly  
63 unperturbed at synapses lacking *Esy1* expression. However, presynaptic overexpression of *Esy1*  
64 leads to enhanced synaptic growth, neurotransmission, and sustainment of the vesicle pool  
65 during intense levels of activity, suggesting that elevated *Esy1* at the ER promotes constitutive  
66 membrane trafficking or lipid exchange with the plasma membrane. Finally, we find that *Esy1*  
67 mutants fail to maintain basal neurotransmission and short term plasticity at elevated  
68 extracellular  $\text{Ca}^{2+}$ , consistent with *Esy1* functioning as an ER  $\text{Ca}^{2+}$  sensor that modulates  
69 synaptic activity. Thus, we identify *Esy1* as a presynaptic ER  $\text{Ca}^{2+}$  sensor that can promote  
70 neurotransmission and synaptic growth, revealing the first *in vivo* neuronal functions of this  
71 conserved gene family.

72

73

74

75

76

77

## 78 INTRODUCTION

79 The endoplasmic reticulum (ER) is a continuous intracellular organelle with critical but enigmatic  
80 roles at synapses. The ER in neurons is involved in diverse functions including synthesis,  
81 modification, and trafficking of proteins and lipids, as well as local regulation of  $\text{Ca}^{2+}$   
82 homeostasis (Renvoise and Blackstone, 2010; Kwon et al., 2016). Indeed, the importance of  
83 synaptic ER is further underscored by its involvement in human disease, including hereditary  
84 spastic paraplegias (Montenegro et al., 2012; Noreau et al., 2014), amyotrophic lateral sclerosis  
85 (Yang et al., 2009; Fasana et al., 2010), Parkinson's disease (Stutzmann and Mattson, 2011),  
86 and Alzheimer's disease (Zhang et al., 2009; Stutzmann and Mattson, 2011). At presynaptic  
87 terminals, recent studies have established important roles for the ER in both membrane  
88 trafficking and  $\text{Ca}^{2+}$  signaling. These studies have revealed that constitutive membrane  
89 trafficking is guided through presynaptic ER to the plasma membrane, necessary for the  
90 delivery of transmembrane and secreted proteins required for synaptic growth and maintenance  
91 (Pfenninger, 2009; Ramirez and Couve, 2011). In addition, presynaptic ER tightly regulates  
92 local  $\text{Ca}^{2+}$  dynamics by orchestrating  $\text{Ca}^{2+}$  release and sequestration at the ER (Bardo et al.,  
93 2006; Kwon et al., 2016). However, it is unclear whether and how presynaptic ER modulates  
94 synaptic strength during synaptic activity.

95 Extended Synaptotagmins (Esyts) are a family of  $\text{Ca}^{2+}$  sensitive proteins that are  
96 attractive candidates to function as ER  $\text{Ca}^{2+}$  sensors that modulates local  $\text{Ca}^{2+}$  dynamics. Esyts  
97 are defined by the presence of a hydrophobic stretch (HS) followed by a synaptotagmin-like  
98 mitochondrial lipid binding protein (SMP) domain and multiple  $\text{Ca}^{2+}$ -binding  $\text{C}_2$  domains and  
99 were recently identified as evolutionarily conserved from yeast (Tricalbin1-3) through mammals  
100 (Esyts1-3) (Min et al., 2007; Manford et al., 2012; Herdman and Moss, 2016). Esyts are targeted  
101 to the ER by a HS and can mediate tethering of ER-plasma membrane (PM) contact sites to  
102 facilitate ER-PM lipid transfer (Giordano et al., 2013; Saheki et al., 2016; Yu et al., 2016; Saheki  
103 and De Camilli, 2017), while other functions for Esyts have also been proposed (Jean et al.,

104 2010; Jean et al., 2012; Tremblay et al., 2015). Interestingly, this membrane tethering and lipid  
105 transfer activity by *Esy1* is only activated upon elevated intracellular concentrations of  $\text{Ca}^{2+}$   
106 suggesting that *Esy1* is a low affinity  $\text{Ca}^{2+}$  sensor that may only be activated during specific  
107 conditions of elevated  $\text{Ca}^{2+}$ , such as store-operated  $\text{Ca}^{2+}$  entry and/or neurotransmission  
108 (Idevall-Hagren et al., 2015). However, a recent study reported no apparent changes in ER  
109 morphology or function at synapses in mutant mice lacking all three *Esy1* isoforms (Sclip et al.,  
110 2016), raising questions about what functions, if any, *Esy1*s may have at synapses.

111         The fruit fly *Drosophila melanogaster* is a powerful model system to elucidate the in vivo  
112 functions of *Esy1*. In contrast to mammals, there is a single, highly conserved *Esy1* ortholog.  
113 Further, the fly neuromuscular junction (NMJ) enables an array of imaging, electrophysiological,  
114 and genetic approaches to illuminate the fundamental roles of genes at synapses. We have  
115 therefore generated and characterized the first *Esy1* mutations in *Drosophila* to test the role of  
116 *Esy1* in synaptic growth, function, and plasticity. Specifically, we examined synapses lacking and  
117 overexpressing *Esy1* at basal states and under synaptic stress. We find that *Esy1* localizes to an  
118 extensive presynaptic ER network. We also find no significant changes in the levels of synaptic  
119 phospholipids, nor do we observe major defects in synaptic growth, function, or plasticity, in  
120 *Esy1* mutants. However, we find that *Esy1* is necessary for proper neurotransmission and short-  
121 term synaptic plasticity at elevated extracellular  $\text{Ca}^{2+}$  levels, consistent with *Esy1* functioning as  
122 a low affinity ER  $\text{Ca}^{2+}$  sensor. Furthermore, presynaptic overexpression of *Esy1* promotes  
123 synaptic growth, transmission, and sustainment of a functional vesicle pool during intense  
124 synaptic activity, suggesting that an increased supply of synaptic membrane due to *Esy1*  
125 overexpression may facilitate synaptic growth and vesicle biogenesis. Thus, *Esy1* is a  
126 presynaptic ER  $\text{Ca}^{2+}$  sensor required for transmission at elevated  $\text{Ca}^{2+}$  levels, which can  
127 promote synaptic growth when expressed at elevated levels.

128

## 129 MATERIALS AND METHODS

### 130 Fly stocks

131 All *Drosophila* stocks were raised at 25°C on standard molasses food. The *w*<sup>1118</sup> strain is used  
132 as the wild-type control unless otherwise noted, as this was the genetic background into which  
133 all genotypes and transgenic lines were crossed. The *Drosophila* stocks used in this study are  
134 following: *OK6-Gal4* (Aberle et al., 2002), *BG57-Gal4* (Budnik et al., 1996), *UAS-GFP-KDEL*  
135 (Dong et al., 2013; Nandi et al., 2014), *UAS-GFP-myc-2xFYVE* (Wucherpennig et al., 2003),  
136 *UAS-PH-PLCδ1-GFP* (Verstreken et al., 2009; Khuong et al., 2010). The *Esy<sup>l</sup>* mutant  
137 (*Mi{ET1}Esy<sup>l</sup>2<sup>MB029221</sup>*), the *Esy<sup>t</sup>* deficiency (*Df(3R)Exel7357*), and all other stocks were obtained  
138 from the Bloomington *Drosophila* Stock Center unless otherwise noted. Standard crossing  
139 strategies and chromosomal balancers were used. Female larvae were used unless otherwise  
140 specified.

141

### 142 Molecular biology

143 *Esy<sup>t</sup>* cDNA (RE26910) was obtained as an expressed sequence tag from the *Drosophila*  
144 Genomics Resources Center. Full-length *Esy<sup>t</sup>* cDNA was PCR amplified using the following  
145 primers: F: 5' CGGCGGTACCCAAAATGAGCGATAACAGTC 3' and R: 5'  
146 CTACATATGAGCCACCGCCCTCGTGCCGTATTTTCAG 3'. The PCR products were subcloned  
147 into the pACU2 vector (Han et al., 2011). An mCherry or 3xFlag tag were inserted in-frame at  
148 the C-terminal end of the pACU2-*Esy<sup>t</sup>* construct. To generate *Esy<sup>t</sup>Δ<sup>HS</sup>*, the *Drosophila Esy<sup>t</sup>*  
149 hydrophobic stretch was identified by the SMART domain online tool ([http://smart.embl-](http://smart.embl-heidelberg.de/)  
150 [heidelberg.de/](http://smart.embl-heidelberg.de/)). *Esy<sup>t</sup>* coding DNA before and after the identified hydrophobic stretch were  
151 separately PCR amplified and ligated into the pACU2-*mCherry* vector using the Gibson  
152 Assembly Cloning Kit (New England Biolabs Inc., E5510S). Finally, for cloning of pACU2-*Esy<sup>t</sup><sup>D</sup>*  
153 <sup>N</sup>, the conserved aspartates in each C<sub>2</sub> domains were identified and mutated into asparagine  
154 (D364N, D374N, D421N, D423N, E429Q for C<sub>2</sub>A; D517N, D564N for C<sub>2</sub>B; D746N, D752N for

155 C<sub>2</sub>C) by synthesizing and inserting a stretch of DNA that covered the entire C<sub>2</sub> domain region.  
156 All constructs were sequenced to verify accuracy, and injected into the VK18 recombination site  
157 on the second chromosome by BestGene Inc (Chino Hill, CA).

158 *Esy<sup>t</sup>* mutants were generated using a CRISPR/Cas9 genome editing strategy as  
159 described (Gratz et al., 2013b; Gratz et al., 2013a; Yu et al., 2013; Bassett and Liu, 2014;  
160 Beumer and Carroll, 2014; Sebo et al., 2014). Briefly, a target Cas-9 cleavage site in *Esy<sup>t</sup>* was  
161 chosen using the CRISPR optimal target finder  
162 (<http://tools.flycrispr.molbio.wisc.edu/targetFinder/>). The earliest target in the first common exon  
163 shared by all putative *Esy<sup>t</sup>* isoforms without any obvious off target sequences in the *Drosophila*  
164 genome was chosen (sgRNA target sequence: 5'GACAAATGGAAACTCAATTGTGG3', PAM  
165 underscored). DNA sequences covering this target sequence were synthesized and subcloned  
166 into the pU6-BbsI-chiRNA plasmid (Addgene 45946) at the BbsI restriction enzyme digestion  
167 site. To generate the sgRNA, pU6-BbsI-chiRNA was PCR amplified using the following primers:  
168 F: 5' GGCGAATTGGGTACCGGG 3' and R: 5' CTGCAGGAATTCGATAAAAAAGCACC 3' and  
169 cloned into the pattB vector (Bischof et al., 2007). The construct was injected into the VK18  
170 insertion sequence and balanced. 20 lines were generated and sequenced to screen for  
171 putative disruptions in the *Esy<sup>t</sup>* locus. 17/20 lines produced a deletion or insertion that led to  
172 frameshift mutations. The line which produced the earliest stop codon (K32stop) was chosen for  
173 further analyses and named the *Esy<sup>t</sup>* allele.

174

## 175 **Immunocytochemistry**

176 Wandering third-instar larvae were dissected in ice cold 0 Ca<sup>2+</sup> modified HL3 saline (Stewart et  
177 al., 1994; Dickman et al., 2005) containing (in mM): 70 NaCl, 5 KCl, 10 MgCl<sub>2</sub>, 10 NaHCO<sub>3</sub>, 115  
178 Sucrose, 5 Trehalose, 5 HEPES, pH 7.2, and immunostained as described (Dickman et al.,  
179 2006). Briefly, larvae were washed three times with modified HL3 saline, and fixed in either  
180 Bouin's fixative (Sigma, HT10132-1L) or 4% paraformaldehyde in PBS (Sigma, F8775). Larvae

181 were washed with PBS containing 0.1% Triton X-100 (PBST) and incubated in primary  
182 antibodies at 4°C overnight. The larvae were then washed in PBST and incubated in secondary  
183 antibodies at room temperature for two hours. Samples were transferred in VectaShield (Vector  
184 Laboratories) and mounted on glass cover slides. The following antibodies were used: mouse  
185 anti-Bruchpilot (BRP; nc82; 1:100; Developmental Studies Hybridoma Bank; DSHB); affinity-  
186 purified rabbit anti-GluRIII (1:2000; (Marrus et al., 2004; Chen et al., 2017), mouse anti-Flag  
187 (1:500; F1804; Sigma-Aldrich), guinea pig anti-vGlut (1:2000; (Daniels et al., 2004; Chen et al.,  
188 2017)), mouse anti-FasII (1:20; 1D4; DSHB), mouse anti-GFP (1:1000; 3e6; Thermo Fisher  
189 Scientific). Alexa Fluor 647-conjugated goat anti-HRP (Jackson ImmunoResearch) was used at  
190 1:200. Donkey anti-mouse and anti-rabbit Alexa Fluor 488-, Cy3, and Rhodamine Red X  
191 secondary antibodies (Jackson ImmunoResearch) were used at 1:400.

192

### 193 **Confocal imaging and analysis**

194 Larval muscles 4 of abdominal segments A2 and A3 were imaged on a Nikon A1R resonant  
195 scanning confocal microscope using a 100x APO 1.4NA oil immersion objective with NIS  
196 Elements software as described (Chen et al., 2017). The fluorescence signals were excited by  
197 separate channels with laser lines of 488 nm, 561 nm, and 637 nm. Images were acquired using  
198 identical settings optimized for signal detection without saturation of the signal for all genotypes  
199 within an experiment. The general analysis toolkit in the NIS Elements software was used to  
200 quantify bouton number, BRP and GluRIII puncta number, and density by applying intensity  
201 thresholds on each of the three channels. For live imaging of *Esyt<sup>mChe</sup>*, wandering third-instar  
202 larvae were dissected, washed, and incubated in Alexa Fluor 647-conjugated goat anti-HRP in 0  
203  $\text{Ca}^{2+}$  modified HL3 at 1:200 for 5 min. The samples were then washed and covered in 0  $\text{Ca}^{2+}$   
204 modified HL3 saline and mounted on glass cover slides. Images were acquired and analyzed as  
205 described above.



206 FM1-43 experiments were performed as described (Dickman et al., 2005). Briefly, larvae  
207 were dissected in ice-cold 0 Ca<sup>2+</sup> modified HL3 and washed, then stimulated for 10 min with a  
208 modified HL3 solution containing 90 mM mM KCl and 10 μM FM1-43 (Molecular Probes,  
209 Eugene, Oregon). Larvae were then washed in 0 Ca<sup>2+</sup> saline before imaging. Images were  
210 acquired using a Nikon A1R confocal microscope using a 60x APO 1.0NA water immersion  
211 objective and imaged as described above. The general analysis toolkit in the NIS Elements  
212 software was used to quantify the mean intensity by applying intensity thresholds.

213

### 214 **Western blotting**

215 Third-instar larval CNS extracts (50 animals of each genotype) and adult heads (7 of each  
216 genotype) were homogenized in ice cold lysis buffer (10 mM HEPES + 150 mM NaCl, pH 7.4),  
217 mixed with an EDTA-free protease inhibitor cocktail (Roche), and run on 4-12% Bis Tris Plus  
218 gels (Invitrogen). After blotting onto PVDF membrane (Novex) and incubation with 5% nonfat  
219 milk in TBST (10 mM Tris, pH 8.0, 150 mM NaCl, 0.5% Tween 20) for 60 min, the membrane  
220 was washed once with TBST and incubated with anti-Esyt (1:2000) and anti-actin (1:2000;  
221 JLA20, DSHB) antibodies overnight at 4C. Membranes were washed and incubated with a  
222 1:5000 dilution of horseradish peroxidase-conjugated secondary antibodies (Jackson  
223 ImmunoResearch) for 1 h. Blots were washed with TBST and developed with the ECL Plus  
224 Western Blotting system (HyGLO). To generate Esyt polyclonal antibodies, a peptide antigen  
225 was synthesized consisting of amino acids 799-816 of Esyt (CTQTGLNSWFDLQPEIRHE). This  
226 peptide was conjugated to KLH and injected into two rabbits (Cocalico Inc, Pennsylvania). The  
227 rabbit immunosera was affinity purified and used at 1:2000.

228

### 229 **Electron microscopy**

230 EM analysis was performed as described (Atwood et al., 1993). Wandering third-instar larvae  
231 were dissected in Ca<sup>2+</sup>-free HL3, then fixed in 2.5% glutaraldehyde/0.1M cacodylate buffer at

232 4C. Larvae were then washed in 0.1M cacodylate buffer. The whole mount of body wall  
233 musculature were placed in 1% osmium tetroxide/0.1M cacodylate buffer at room temperature  
234 for 1hr. After washing, larvae were then dehydrated in Ethanol. Samples were cleared in  
235 propylene oxide and infiltrated with 50% Eponate 12 in propylene oxide overnight. The following  
236 day, samples were embedded in fresh Eponate 12. Electron micrographs were obtained on a  
237 Morgagni 268 transmission electron microscope (FEI, Hillsboro, OR). The junctional region was  
238 serially sectioned at a thickness of 60-70 nm. The sections were stained in 2% uranyl acetate  
239 for 3 minutes, washed briefly 3x in distilled water, stained in Reynolds lead citrate for 1 minute,  
240 washed briefly 3x in distilled water and dried. Sections were mounted on Formvar coated single  
241 slot grids. Larval muscles 6/7 of abdominal segments were viewed at a 23,000x magnification,  
242 and recorded with a Megaview II CCD camera. Images were analyzed blind to genotype using  
243 the general analysis toolkit in the NIS Elements software.

244

## 245 **Electrophysiology**

246 All dissections and recordings were performed in modified HL3 saline with 0.4 CaCl<sub>2</sub> (unless  
247 otherwise specified). Larvae were dissected and washed several times with modified HL3  
248 saline. Sharp electrode intracellular recordings (electrode resistance between 10-35 MΩ) were  
249 performed on muscles 6 of abdominal segments A2 and A3 as described (Chen et al., 2017).  
250 Recordings were acquired using an Axoclamp 900A amplifier, Digidata 1440A acquisition  
251 system and pClamp 10.5 software (Molecular Devices). Electrophysiological sweeps were  
252 digitized at 10 kHz, and filtered at 1 kHz. Miniature excitatory postsynaptic potentials (mEPSPs)  
253 were recorded for one min in the absence of any stimulation. Excitatory postsynaptic potentials  
254 (EPSPs) were recorded while cut motor axons were stimulated using an ISO-Flex stimulus  
255 isolator (A.M.P.I.). Intensity was adjusted for each cell, set to consistently elicit responses from  
256 both neurons innervating the muscle segment, but avoiding overstimulation. Data were  
257 analyzed using Clampfit (Molecular devices), MiniAnalysis (Synaptosoft), Excel (Microsoft), and

258 SigmaPlot (Systat) software. Average mEPSP, EPSP, and quantal content were calculated for  
259 each genotype with and without corrections for nonlinear summation (Martin, 1955). Recordings  
260 were rejected when muscle input resistance ( $R_{in}$ ) was less than 3 M $\Omega$ , and resting membrane  
261 potential ( $V_{rest}$ ) was above -60 mV or if either measurement deviated by more than 10% during  
262 the course of the experiment. To acutely block postsynaptic receptors, larvae with intact motor  
263 nerves were dissected and incubated with or without philanthotoxin-433 (PhTx; Sigma; 20  $\mu$ M)  
264 for 10 min. Larvae were resuspended in modified HL3, and motor nerves were cut as described  
265 (Frank et al., 2006; Dickman and Davis, 2009). For TEVC, muscles were clamped to -70 mV  
266 and stimulus train of 4 EPSC pulses were evoked with a 60 Hz, 0.5 msec stimulus duration,  
267 while recording in 3 mM Ca<sup>2+</sup> modified HL3. Short-term plasticity was estimated by dividing the  
268 fourth EPSC with the first EPSC. Data were analyzed as described above.

269

## 270 **Statistical Analysis**

271 All data are presented as mean +/-SEM. Data were compared using either a one-way ANOVA  
272 and tested for significance using a 2-tailed Bonferroni post-hoc test, or using a Student's t-test  
273 (where specified) with Graphpad Prism or Microsoft Excel software, and with varying levels of  
274 significance assessed as  $p < 0.05$  (\*),  $p < 0.01$  (\*\*),  $p < 0.001$  (\*\*\*), ns=not significant. Quantal  
275 content was calculated for each individual recording using the equation  $QC = EPSP/mEPSP$ .  
276 The QC was corrected for non-linear summation for the Ca<sup>2+</sup>-cooperativity analysis, using the  
277 equation  $QC_{corrected} = (EPSP/mEPSP)(1-EPSP/V_0)^{-1}$  where  $V_0 = (\text{reversal potential} - \text{resting}$   
278  $\text{potential})$  (Martin, 1955). Full statistical details and information can be found in Table 1.

279

## 280 **Data availability**

281 Fly stocks are available upon request. Table 1 contains genotypes used and full statistical  
282 details for each figure.

283

## 284 RESULTS

### 285 Generation of null mutations in *Drosophila Esyt*

286 The rodent genome encodes three *extended synaptotagmin* isoforms (*Esy1*, *Esy2*, and *Esy3*;  
287 (Min et al., 2007)). *Esy1* encodes five C<sub>2</sub> domains, while *Esy2* and *Esy3* each contain three  
288 (Fig 1B). In contrast, the *Drosophila* genome encodes a single *Esy* ortholog, which is most  
289 similar to mouse *Esy2* by amino acid sequence (54% similar, 34% identical). There are four  
290 predicted *Esy* isoforms based on expressed sequence tags ([www.flybase.org](http://www.flybase.org)). However, only  
291 one transcript (*Esy2-RB*) appears to be the major isoform based on the expression profile.  
292 RNA-seq data suggests *Esy* is expressed in embryonic stages after 10h through adults in all  
293 tissues examined, consistent with *Esy* being ubiquitously expressed. We generated null  
294 mutations in the *Drosophila Esyt* gene using CRISPR/Cas-9 genome editing technology (Gratz  
295 et al., 2013b; Gratz et al., 2013a; Yu et al., 2013; Bassett and Liu, 2014; Beumer and Carroll,  
296 2014; Sebo et al., 2014). Screening of 20 lines with active CRISPR mutagenesis led to 17 with  
297 independent deletions or insertions with predicted frameshift mutations in the *Esy* open reading  
298 frame (see methods). We chose one such mutation for further study, *Esy<sup>t1</sup>*, which is predicted to  
299 generate a stop codon at position 32, truncating the *Esy* protein before the hydrophobic stretch  
300 (Fig 1A and 1B). In addition, we obtained a separate *Esy* mutation (*Esy<sup>t2</sup>*), containing a MiMIC  
301 transposon insertion in the first coding intron. This transposon has a gene trap cassette (Venken  
302 et al., 2011; Nagarkar-Jaiswal et al., 2015) that is predicted to truncate the *Esy* transcript by  
303 introducing a stop codon at the second amino acid (Fig 1A and 1B). We generated a polyclonal  
304 antibody against a C-terminal stretch of the *Drosophila Esyt* protein, which recognized an  
305 immunoblot band at ~90 kDa (Fig 1C and 1D), consistent with the predicted molecular mass of  
306 *Esy*. We confirmed that *Esy* is expressed in the adult brain and larval CNS, and that *Esy<sup>t1</sup>* and  
307 *Esy<sup>t2</sup>* are protein null mutations by immunoblot analysis (Fig 1C and 1D). Finally, we generated  
308 a series of transgenic *Esy* constructs under *UAS* control for further analysis (Fig 1B). We  
309 engineered a full length *Esy* transgene (*Esy2-RB* isoform) tagged with both mCherry and

310 3xFlag tags ( $\text{Esyt}^{\text{mCh}}$ ), and a separate transgene tagged with only a 3xFlag tag ( $\text{Esyt}^{\text{Flag}}$ ). For  
311 structure/function studies, we also generated an *Esyt* transgene without the conserved  
312 hydrophobic stretch ( $\text{Esyt}^{\Delta\text{HS}}$ ), predicted to disrupt membrane targeting of Esyt (Giordano et al.,  
313 2013), and specifically mutated each  $\text{C}_2$  domain to render them unable to bind to  $\text{Ca}^{2+}$  ( $\text{Esyt}^{\text{D-N}}$ ;  
314 see methods). Using these reagents, we went on to determine the presynaptic localization of  
315 Esyt.

316

### 317 **The hydrophobic stretch anchors Esyt to axonal ER**

318 In neurons, the ER is an extensive network present in the somatic perinucleus as well as in  
319 distal dendrites and axons (Terasaki et al., 1994; Spacek and Harris, 1997; Meldolesi, 2001;  
320 Verkhatsky, 2005; Bardo et al., 2006; Wang et al., 2007; Blackstone et al., 2011; O'Sullivan et  
321 al., 2012; Wong et al., 2014; Summerville et al., 2016). Given that ER proteins can have uniform  
322 or heterogeneous localization in the elaborate ER network (Chang and Liou, 2016), we sought  
323 to determine the subcellular localization of *Drosophila* Esyt at presynaptic terminals. We were  
324 unable to obtain specific immunolabeling against endogenous Esyt using the antibody we  
325 generated. Therefore, we expressed tagged *Esyt* constructs in motor neurons.  $\text{Esyt}^{\text{mCh}}$  trafficked  
326 to presynaptic terminals, where it invaded synaptic boutons and co-localized with an established  
327 ER marker, the ER retention signal KDEL fused to GFP (*GFP-KDEL*; Fig 2A; (Dong et al., 2013;  
328 Nandi et al., 2014)). Next, we tested whether Esyt localization and trafficking to ER was  
329 dependent on the hydrophobic stretch (HS) domain and on  $\text{Ca}^{2+}$  binding to the  $\text{C}_2$  domains.  
330 Previous studies have shown that the HS domain tethers Esyt to the ER, while deletion of the  
331 HS domain shifts Esyt localization to the cytosol and plasma membrane (Min et al., 2007;  
332 Giordano et al., 2013). We therefore expressed the mCherry-tagged Esyt construct lacking the  
333 HS domain in neurons ( $\text{Esyt}^{\Delta\text{HS}}$ ; see Fig 1B and methods). As expected, the  $\text{Esyt}^{\Delta\text{HS}}$  signal was  
334 no longer restricted to the axonal ER, and instead filled the presynaptic terminal, indicating a  
335 shift to cytosolic localization (Fig 2B). We next tested the requirement of  $\text{Ca}^{2+}$  binding for Esyt

336 trafficking and localization by expressing *Esy<sup>D-N</sup>*, which lacks the negatively charged amino  
337 acids in each C<sub>2</sub> domain required for Ca<sup>2+</sup> binding. Interestingly, we were unable to detect any  
338 *Esy<sup>D-N</sup>* signal at synaptic terminals (Fig 2C and 2D). Instead, most of the *Esy<sup>D-N</sup>* signal was  
339 restricted to the cell body (data not shown). This indicates that trafficking of *Esy<sup>D-N</sup>* to synaptic  
340 terminals requires the ability to bind Ca<sup>2+</sup>. However, we cannot exclude the possibility that the  
341 D-N mutations might have resulted in misfolding of the protein, potentially disrupting trafficking  
342 or stability. We also found that expression of the *Esy<sup>D-N</sup>* transgene led to embryonic lethality  
343 when driven pan-neuronally or in muscle. This is not unexpected, as others have observed that  
344 Synaptotagmin expression with similar mutations to C<sub>2</sub> domains acquired a lethal toxicity  
345 (Mackler et al., 2002). Together, these data demonstrate that *Drosophila* *Esy<sup>D-N</sup>* is localized to  
346 presynaptic ER structures through the HS domain and that Ca<sup>2+</sup> binding to *Esy<sup>D-N</sup>* appears to be  
347 required for *Esy<sup>D-N</sup>* trafficking in neurons.

348         Given that *Esy<sup>D-N</sup>* localizes to axonal ER, we examined the morphology of the ER network  
349 at synaptic terminals with loss or overexpression of *Esy<sup>D-N</sup>*. Expression of *GFP-KDEL* alone in  
350 motor neurons labeled an extensive presynaptic network extending throughout synaptic  
351 boutons, as observed by others (data not shown; (Summerville et al., 2016)). This network did  
352 not appear to be perturbed in *Esy<sup>D-N</sup>* mutants, nor with overexpression (data not shown). These  
353 results suggest that ER structure and elaboration is not dependent on *Esy<sup>D-N</sup>* expression. Lastly,  
354 we found that the ER network labeled by *Esy<sup>D-N</sup>* is localized near, but distinct from, other synaptic  
355 compartments including active zones, synaptic vesicle pools, periaxonal regions, and the  
356 neuronal plasma membrane (Fig 2E and 2F). Thus, *Esy<sup>D-N</sup>* is localized to the presynaptic ER  
357 network and present near areas of synaptic vesicle fusion and recycling at presynaptic terminals  
358 where it could, in principle, modulate synaptic structure and function.

359

360 **Synaptic phospholipid balance does not require *Esy<sup>D-N</sup>***

361 Given that *Esy1* has been implicated in phospholipid transfer and homeostasis in non-neuronal  
362 cells, we next sought to determine whether the level and distribution of phospholipids at  
363 presynaptic terminals was altered in *Esy1* mutants and/or with overexpression of *Esy1* in motor  
364 neurons (*Esy1*-OE). The phospholipid phosphatidylinositol 4,5-bisphosphate (PI(4,5)P<sub>2</sub>) plays  
365 crucial roles at presynaptic terminals, regulating synaptic protein-protein interactions, ion  
366 channel biophysics, neurotransmission, and synaptic vesicle trafficking (De Camilli et al., 1996;  
367 Lemmon, 2003; Di Paolo et al., 2004; Di Paolo and De Camilli, 2006; Slabbaert et al., 2012;  
368 Lauwers et al., 2016). To determine levels of PI(4,5)P<sub>2</sub>, we expressed a fluorescently tagged  
369 pleckstrin homology domain of phospholipase C- $\delta$ 1 (PLC $\delta$ 1-PH-GFP) that specifically labels  
370 PI(4,5)P<sub>2</sub> (Verstreken et al., 2009; Khuong et al., 2010; Chen et al., 2014). Expression of this  
371 transgene in motor neurons revealed specific labeling of the plasma membrane at presynaptic  
372 terminals, consistent with the expected distribution of PI(4,5)P<sub>2</sub> (Fig 3A). When *PLC $\delta$ 1-PH-GFP*  
373 was expressed in *Esy1* mutants, we were unable to detect any difference in intensity or  
374 distribution, nor did PLC $\delta$ 1-PH-GFP levels change with *Esy1*-OE (Fig 3A and 3B). Thus, we find  
375 no evidence that PI(4,5)P<sub>2</sub> levels or distribution is altered at synapses with gain or loss of *Esy1*  
376 expression.

377 In addition to the plasma membrane, the ER also associates with early and late  
378 endosomal structures (Rowland et al., 2014; Raiborg et al., 2015; Eden, 2016; Phillips and  
379 Voeltz, 2016). ER-endosome contact sites modulate endosomal structure and function,  
380 contributing to synaptic growth and vesicle trafficking (Wucherpfennig et al., 2003; Rowland et  
381 al., 2014; Raiborg et al., 2015). Thus, we considered the possibility that *Esy1* may regulate lipid  
382 transfer or otherwise influence endosomes at synapses. In particular, we focused on early  
383 endosomes known to be involved in synaptic vesicle trafficking and recycling. These early  
384 endosomes are specifically labeled by the small GTPase Rab5 and are enriched in the  
385 phospholipid phosphatidylinositol-3-phosphate (PI(3)P) (Wucherpfennig et al., 2003; Rodal et  
386 al., 2011; Slabbaert et al., 2012). The FYVE finger domain of the Rab5 effectors EEA1 and

387 Rabenosyin-5 bind specifically to PI(3)P, which is an established marker for early endosomes  
388 (Stenmark et al., 1995; Simonsen et al., 1998; Lawe et al., 2000; Wucherpfennig et al., 2003).  
389 To test if PI(3)P levels and/or distribution are dependent on *Esyt* expression, we expressed a  
390 GFP-fused FYVE domain transgene (*GPF-myc-2xFYVE*) in *Esyt* mutants and *Esyt*-OE. GFP-  
391 myc-2xFYVE expression in controls labeled a punctate structure in presynaptic boutons, as  
392 expected (Fig 3C). However, we observed no differences in the intensity of GFP-myc-2xFYVE  
393 in *Esyt* mutants and *Esyt*-OE compared to control (Fig 3C and 3D). Thus, we find no evidence  
394 that *Esyt* is involved in phospholipid balance, transfer, or distribution at presynaptic terminals.  
395

### 396 **Presynaptic overexpression of *Esyt* promotes synaptic growth and transmission**

397 Axonal ER plays a critical role in synaptic growth and neurotransmission in mammals and  
398 *Drosophila* (Verkhatsky, 2005; Wang et al., 2007; Pfenninger, 2009; Renvoise and Blackstone,  
399 2010; Blackstone et al., 2011; O'Sullivan et al., 2012; Petkovic et al., 2014; Wong et al., 2014;  
400 Kwon et al., 2016; Summerville et al., 2016; de Juan-Sanz et al., 2017). Indeed, recent studies  
401 have demonstrated that loss of the genes *atlastin* or *reticulon2*, involved in ER membrane fusion  
402 and tube formation, respectively, leads to axonal ER fragmentation and results in increased  
403 synaptic growth and decreased neurotransmitter release at the *Drosophila* NMJ (Wang et al.,  
404 2007; Blackstone et al., 2011; O'Sullivan et al., 2012; Summerville et al., 2016). We therefore  
405 sought to determine to what extent *Esyt* expression contributes to synaptic development and  
406 neurotransmission. First, we quantified synaptic growth by immunostaining NMJs with  
407 antibodies that recognize neuronal membrane (HRP), active zones (BRP), and postsynaptic  
408 glutamate receptors (DGluRIII). *Esyt* mutants exhibited no significant differences in the number  
409 of synaptic boutons, nor in the number or density of active zones or glutamate receptor clusters  
410 at the NMJ (Fig 4A, 4B, 4D, and 4E). However, overexpression of two independent *Esyt*  
411 transgenes in motor neurons, *Esyt*<sup>mCh</sup> and *Esyt*<sup>Flag</sup>, revealed a ~40% increase in synaptic  
412 growth, including increased neuronal membrane surface area and total number of active zones



413 per NMJ (Fig 4A-4D). Thus, while loss of *Esyt* has no apparent impact on synaptic growth or  
414 structure, elevated levels of *Esyt* in motor neurons promotes synaptic growth at the NMJ.

415         Given that *Esyt*-OE promotes synaptic growth, we next assessed whether parallel  
416 changes in neurotransmission are observed with loss or enhanced expression of *Esyt*. We  
417 observed no significant differences in synaptic physiology at lowered extracellular  $\text{Ca}^{2+}$  (0.4 mM)  
418 in *Esyt* mutants compared with controls (Fig 5A-D). In particular, there were no significant  
419 changes in mEPSP amplitude, EPSP amplitude, or quantal content (Fig 5A-5D). However, in  
420 these conditions, *Esyt*-OE exhibited a mild increase in EPSP amplitude and quantal content,  
421 without any significant difference in mEPSP amplitude (Fig 5A-5D). The increased growth  
422 observed in *Esyt*-OE may contribute to this enhancement of synaptic strength, although clearly  
423 there is less change than might be predicted by the increase in growth. Thus, while *Esyt*  
424 mutants have no obvious defects in synaptic growth, structure, or transmission, *Esyt*-OE  
425 promotes growth and function.

426         Finally, we tested whether *Esyt* was necessary to sustain synaptic transmission during  
427 elevated periods of activity. During high frequency stimulation at the *Drosophila* NMJ,  
428 endocytosis rates must be increased to sustain the elevated level of exocytosis, and any  
429 imbalance in this coupling will lead to depletion of the functional vesicle pool (Verstreken et al.,  
430 2002; Verstreken et al., 2003; Dickman et al., 2005; Haucke et al., 2011). We utilized a  
431 previously established protocol, in which we subject the NMJ to 10 Hz stimulation at elevated  
432 extracellular  $\text{Ca}^{2+}$  for 10 min, followed by recovery for an additional 10 min, taking a test pulse at  
433 0.2 Hz (Verstreken et al., 2002; Dickman et al., 2005). This analysis revealed that wild type and  
434 *Esyt*-mutant synapses exhibited a similar rate of vesicle pool depletion and recovery, finishing at  
435 ~30% of the original EPSP amplitude, followed by a recovery to ~60% of the initial value (Fig  
436 5E). In both genotypes, a similar number of total quanta were released (Fig 5F). In contrast,  
437 *Esyt*-OE conferred a resistance to depletion of the functional synaptic vesicle pool as well as  
438 enhanced recovery. 10 Hz stimulation of *Esyt*-OE NMJs revealed a slower rate of rundown and

439 faster recovery of the depleted vesicle pool (Fig 5E), finishing at ~60% and recovering to ~90%  
440 of starting EPSP amplitudes. Indeed, more total quanta were released in *Esyt*-OE compared to  
441 both wild type and *Esyt* mutants during this sustained period of activity (Fig 5F). Together, this  
442 demonstrates that while the loss of *Esyt* does not impact synaptic growth, structure,  
443 transmission, or recycling, overexpression of *Esyt* in neurons promotes synaptic growth which,  
444 in turn, appears to contribute to a mild enhancement in synaptic strength while sustaining the  
445 vesicle pool during prolonged activity.

446

#### 447 **Synaptic vesicle density and endocytosis is unchanged in *Esyt* mutants and *Esyt*-OE**

448 The slowed rate of synaptic vesicle pool depletion in *Esyt*-OE described above could, in  
449 principle, be due to an increase in the number of synaptic vesicles participating in exocytosis  
450 and recycling at individual boutons. Alternatively, synaptic vesicle recycling at each bouton may  
451 be the same, and the increased maintenance of the vesicle pool may be due to the increased  
452 number of boutons in *Esyt*-OE. We therefore examined NMJ ultrastructure to determine whether  
453 a change in the density of synaptic vesicles in each bouton was apparent that may suggest an  
454 increased starting vesicle pool in *Esyt*-OE. We did not observe any significant change in the  
455 density or distribution of synaptic vesicles within NMJ boutons or near active zones in *Esyt*-OE  
456 compared with wild type and *Esyt* mutants (Fig 6A-6C). More generally, active zone length, T-  
457 bar morphology, and membrane compartments appear similar in all three genotypes (Fig 6A-  
458 6E). Thus, there is no evidence that *Esyt*-OE results in increased numbers or altered distribution  
459 of synaptic vesicles within NMJ boutons.

460         Despite there being no change in the number of synaptic vesicles per bouton in *Esyt*-OE  
461 NMJs, it is possible that more synaptic vesicles participate in exo-endocytosis during activity  
462 which, in turn, could account for the increased maintenance of the functional vesicle pool. We  
463 therefore measured the pool of vesicles participating in endocytosis during high activity using  
464 the lipophilic dye FM1-43, which is absorbed by newly endocytosed synaptic vesicles from the

465 plasma membrane following exocytosis and is a measure of the number of vesicles participating  
466 in release at each bouton (Dickman et al., 2005; Verstreken et al., 2008; Chen et al., 2014).  
467 Following stimulation, we observed no change in the intensity or localization of the endocytic  
468 vesicle pool labeled by FM1-43 in *Esy*t-OE compared to wild type and *Esy*t mutants (Fig 6F and  
469 6G). Thus we find no evidence that the number or function of synaptic vesicles per bouton is  
470 changed at NMJs in *Esy*t-OE. This therefore suggests that the increase in the total number of  
471 synaptic boutons, coupled with less release per bouton, together accounts for the resistance to  
472 depletion of the vesicle pool in *Esy*t-OE during elevated activity. Consistent with this idea, we  
473 observed a trend of reduced FM1-43 intensity per bouton following activity in *Esy*t-OE (Fig.  
474 6F,G).

475

476 ***Esy*t is necessary for proper presynaptic function and short term plasticity at elevated**  
477 **Ca<sup>2+</sup>**

478 *Esy*t is a putative Ca<sup>2+</sup> sensor localized to axonal ER, but we were unable to observe any  
479 significant roles for *Esy*t in neurotransmission at lowered extracellular Ca<sup>2+</sup>. Indeed, in this  
480 condition, no differences in the apparent Ca<sup>2+</sup> sensitivity of neurotransmission between wild  
481 type, *Esy*t mutants, and *Esy*t-OE were observed when quantal content was assessed across a  
482 range of lowered extracellular Ca<sup>2+</sup> concentrations (Fig 7A). Interestingly, in vertebrates, *Esy*t1  
483 dependent ER-PM tethering is activated only by high cytosolic Ca<sup>2+</sup> concentrations (Idevall-  
484 Hagren et al., 2015; Yu et al., 2016), and we therefore hypothesized that *Esy*t function at  
485 synapses may only be revealed at elevated extracellular Ca<sup>2+</sup>. We therefore assayed  
486 neurotransmission and short-term plasticity at elevated extracellular Ca<sup>2+</sup> concentrations (3 mM)  
487 using a two-electrode voltage clamp configuration. We observed no change in EPSC amplitude  
488 in *Esy*t-OE compared with wild type (Fig 7B and 7C). However, EPSC amplitudes were  
489 significantly reduced in *Esy*t mutants compared with wild type and *Esy*t-OE synapses, which  
490 was rescued by presynaptic expression of *Esy*t (Fig 7B and 7C). Finally, we probed short term

491 synaptic plasticity in *Esyt* mutants by evoking four stimuli at 60 Hz in elevated extracellular  $Ca^{2+}$ .  
492 Given that *Esyt* is a  $Ca^{2+}$  sensor localized to axonal ER, this protocol would test a role for *Esyt*  
493 during rapid changes in presynaptic  $Ca^{2+}$  levels (Muller et al., 2011; Muller et al., 2012; Muller et  
494 al., 2015). Wild type and *Esyt*-OE NMJs exhibited synaptic depression, with the fourth EPSC  
495 finishing at ~60% of the starting EPSC amplitude (Fig 7D). In contrast, *Esyt* mutants showed  
496 reduced depression, finishing at ~90% of the starting EPSC amplitude, which was rescued by  
497 presynaptic *Esyt* expression (Fig 7B and 7D). Together, this data is consistent with a  $Ca^{2+}$   
498 sensing function of *Esyt* at axonal ER in promoting synaptic vesicle release during evoked  
499 activity.

500

#### 501 ***Esyt* has no role in presynaptic homeostatic potentiation**

502 Thus far, we have found that *Esyt* has no apparent role in synaptic growth and structure, but is  
503 required to promote synaptic vesicle release at elevated extracellular  $Ca^{2+}$ . Interestingly,  
504 elevated  $Ca^{2+}$  influx at presynaptic terminals at the *Drosophila* NMJ has been demonstrated to  
505 drive an adaptive form of synaptic plasticity referred to presynaptic homeostatic potentiation  
506 (PHP) (Muller and Davis, 2012; Davis and Muller, 2015). At this synapse, pharmacological or  
507 genetic perturbations to postsynaptic glutamate receptors triggers a precise retrograde increase  
508 in presynaptic release that compensates for reduced receptor functionality, restoring baseline  
509 levels of synaptic strength (Frank, 2014). We hypothesized that *Esyt* may be an axonal ER  $Ca^{2+}$   
510 sensor that promotes vesicle release in response to elevated presynaptic  $Ca^{2+}$  influx during  
511 PHP expression. We assayed acute PHP in *Esyt* mutants and *Esyt*-OE. Application of the  
512 glutamate receptor antagonist philanthotoxin-433 (PhTx; (Frank et al., 2006)) to wild-type NMJs  
513 led to the expected ~50% reduction in mEPSP amplitude but normal EPSP amplitude because  
514 of a homeostatic increase in quantal content (presynaptic release) (Fig 8A and 8B). Similarly,  
515 PhTx reduced mEPSP amplitudes in both *Esyt* mutants and *Esyt*-OE, and both genotypes

516 exhibited a robust increase in quantal content (Fig 8A and 8B). Thus, loss or increased  
517 expression of *Esy1* has no consequence on the acute induction or expression of PHP.

518

## 519 **DISCUSSION**

520 We have generated the first mutations in the single *Drosophila Esy1* ortholog and characterized  
521 the presynaptic localization and functions of this gene at the NMJ. We demonstrate that  
522 *Drosophila Esy1* is localized to an extensive axonal ER network. Although *Esy1* was previously  
523 shown to mediate ER-PM tethering and to promote lipid exchange between the two membranes  
524 in non-neuronal cells, we find no evidence that lipid balance is altered at *Esy1* mutant synapses.  
525 Further, synaptic transmission and homeostatic plasticity are surprisingly unperturbed in the  
526 absence of *Esy1* at lowered extracellular  $Ca^{2+}$  and during sustained levels of synaptic activity. In  
527 contrast, presynaptic overexpression of *Esy1* promotes synaptic growth and, in turn, synaptic  
528 transmission during elevated activity. Finally, we reveal an important function for *Esy1* in  
529 facilitating presynaptic release at elevated  $Ca^{2+}$  levels. Together, our study establishes *Esy1* as  
530 an ER-localized C2 domain protein that regulates synaptic growth when overexpressed and  
531 neurotransmission at elevated  $Ca^{2+}$  levels.

532

### 533 ***Drosophila Esy1* is dispensable for many synaptic functions**

534 *Esy1* is evolutionarily conserved from yeast to humans (Min et al., 2007; Manford et al., 2012),  
535 suggesting this gene family subserves important and fundamental functions that have been  
536 selected for and maintained throughout evolution. Studies in yeast and mammalian cell culture  
537 revealed that *Esy1* mediates lipid transfer at ER-PM contact sites in a  $Ca^{2+}$ -dependent manner  
538 (Saheki et al., 2016; Yu et al., 2016; Saheki and De Camilli, 2017), raising the intriguing  
539 possibility that *Esy1* may modulate lipid metabolism during growth and activity at synapses.  
540 However, recent studies in which all three *Esy1* genes are genetically mutated in mice have  
541 failed to find any apparent defects in viability, fertility, synaptic or ER protein composition, nor in

542 ER/mitochondrial stress responses (Scip et al., 2016; Tremblay and Moss, 2016). Consistent  
543 with these studies, we find that *Esy1* is surprisingly dispensable for lipid balance and  
544 homeostasis at presynaptic terminals, and that synaptic growth, function, and plasticity appear  
545 relatively unperturbed at the *Drosophila* NMJ. We consider two possibilities, not mutually  
546 exclusive, to explain why synapses robustly develop and function in the absence of *Esy1*.

547 First, *Esy1* may participate in such fundamental and essential processes that organisms  
548 may in turn have evolved multiple redundant mechanisms to ensure robustness in these critical  
549 pathways. Indeed, in pioneering work in yeast, the *Esy1* orthologs tricalbins mediate ER-PM  
550 tethering, but this tethering is only disrupted upon loss of three additional ER-PM proteins, *Ist2*,  
551 *Scs2*, and *Scs22*, in addition to the three tricalbins (Manford et al., 2012). This suggests some  
552 level of functional redundancy within and beyond Tricalbin isoforms. Further, a recent study  
553 demonstrated an apparent compensatory increase in expression of the ER-PM tethering  
554 proteins *Orp5*, *Orai1*, and *TMEM110* in *Esy1*, 2, and 3 mutant mice (Tremblay and Moss,  
555 2016). In *Drosophila*, a number of proteins are localized to ER and have been proposed to  
556 contribute to lipid balance and homeostasis in other cellular compartments (Wenk et al., 2003;  
557 Carrasco and Meyer, 2011; Hammond et al., 2014; Dickson et al., 2016). Thus, there is  
558 substantial evidence for a variety of proteins at the ER and other compartments having  
559 potentially redundant function with *Esy1*s.

560 Second, *Esy1* may only have functions revealed in a specific context that was not tested  
561 in our study. We find that *Esy1* is not essential to maintain lipid homeostasis at synapses, at  
562 least for the major phospholipids PI(4,5)P<sub>2</sub> and PI(3)P. This demonstrates that lipid balance and  
563 membrane homeostasis can be maintained during the extreme demands of regulated  
564 membrane trafficking and exchange at presynaptic terminals in the absence of *Esy1*. In  
565 retrospect, this may not be surprising, as a lipid cycle nested within the synaptic vesicle cycle  
566 has long been known to exist at synapses, supported by key synaptic proteins such as  
567 Synaptojanin, Rab5, Minibrain kinase/Dyrk1A, and *Sac1* (De Camilli et al., 1996; Nemoto et al.,

568 2000; Wenk and De Camilli, 2004; Chen et al., 2014). Importantly, there is no known  
569 involvement or requirement for acute lipid transfer from the ER in synaptic vesicle recycling (De  
570 Camilli et al., 1996; Wenk and De Camilli, 2004). Accordingly, lipid homeostasis during synaptic  
571 vesicle trafficking, like protein homeostasis, may be sufficiently embedded and coupled in  
572 membrane trafficking itself so as not to lead to imbalances, even during rapid exo- and endo-  
573 cytos. Thus, a variety of redundant, tissue-specific, and/or specialized functions of *Esy1* likely  
574 explains the relatively subtle effects due to loss of this fundamental gene.

575

### 576 ***Esy1* localizes to axonal ER and promotes neurotransmission at elevated $Ca^{2+}$ levels**

577 We find that *Esy1* is localized to the axonal ER. Further, we demonstrate that *Esy1* promotes  
578 neurotransmission, but only at elevated  $Ca^{2+}$  levels. These findings suggest that *Esy1* may  
579 promote presynaptic function by coupling local  $Ca^{2+}$  dynamics to mechanisms that modulate  
580 intracellular  $Ca^{2+}$  release from the axonal ER. Indeed, axonal ER has emerged as a crucial  
581 organelle that can sense and respond to dynamic change in cytosolic  $Ca^{2+}$  to modulate  
582 presynaptic function and plasticity (Verkhratsky, 2005; Bardo et al., 2006; Kwon et al., 2016; de  
583 Juan-Sanz et al., 2017). For example,  $Ca^{2+}$  influx from the extracellular space can induce  
584 additional  $Ca^{2+}$  release from the ER via ryanodine receptors, a process referred as  $Ca^{2+}$ -induced  
585  $Ca^{2+}$ -release (CICR), which can be activated during single action potentials or during the trains  
586 of stimuli (Verkhratsky, 2005; Bardo et al., 2006; Kwon et al., 2016; de Juan-Sanz et al., 2017).  
587 While the molecular mechanism for how *Esy1* promotes neurotransmission is unclear, it is  
588 unlikely to be through developmental alterations in synaptic structure, since we did not find any  
589 defects in these processes in *Esy1* mutants. Rather, *Esy1* likely has a role at axonal ER in  
590 acutely modulating presynaptic function during activity. An intriguing possibility is that *Esy1* may  
591 work in conjunction with ryanodine receptors as  $Ca^{2+}$  sensors that promotes CICR at the  
592 presynaptic terminal in response to activity. In this model, *Esy1* may respond to elevated  $Ca^{2+}$  at

593 synapses during single action potentials, leading to a supplemental source of presynaptic  $Ca^{2+}$ ,  
594 perhaps through release of intracellular ER stores.

595

### 596 **Esyt, axonal ER, and synaptic growth**

597 Perhaps the most striking and unexpected finding was that elevated expression of *Esyt* in motor  
598 neurons led to increased synaptic growth and a moderate increase in neurotransmission. As  
599 discussed above, we find no evidence that *Esyt* is involved in the regulated membrane  
600 trafficking pathway driving synaptic vesicle recycling. It is therefore attractive to consider that  
601 elevated *Esyt* expression at axonal ER promotes increased membrane trafficking to the plasma  
602 membrane through the constitutive pathway. Indeed, the membrane necessary for synaptic  
603 growth is delivered through the constitutive membrane trafficking pathway, as synapses are  
604 able to form and grow even when toxins are expressed that block or inhibit synaptic vesicle  
605 fusion (Broadie et al., 1995; Sweeney et al., 1995; Dickman et al., 2006; Choi et al., 2014). Of  
606 course, the ER is well established to be a key node in constitutive membrane trafficking to the  
607 PM (Aridor and Fish, 2009; Pfenninger, 2009; Ramirez and Couve, 2011), and increased *Esyt*  
608 expression at axonal ER may facilitate the rate of membrane delivery to the presynaptic  
609 terminal. This, in turn, may lead to excess synaptic growth, as observed in other mutants with  
610 excess presynaptic membrane (Koh et al., 2004; Dickman et al., 2006; O'Connor-Giles et al.,  
611 2008). Thus, the unanticipated finding that increased *Esyt* expression promotes synaptic growth  
612 raises intriguing possibilities for axonal ER perhaps being a rate-limiting step in membrane  
613 delivery at synapses.

614 Our results establish *Esyt* as an axonal ER  $Ca^{2+}$  sensor that promotes presynaptic  
615 function at elevated extracellular  $Ca^{2+}$  levels and may also have unanticipated roles in synaptic  
616 growth. Further work is needed to elucidate the molecular mechanism of how *Esyt* couples  
617 cytosolic  $Ca^{2+}$  to presynaptic ER functions to ultimately modulate transmission and signaling.  
618 While axonal ER was first observed over 40 years ago (Tsukita and Ishikawa, 1976; Ramirez



619 and Couve, 2011), the functions of this complex organelle has remained enigmatic. Recent  
620 studies have begun to reveal how axonal ER sculpts presynaptic Ca<sup>2+</sup> dynamics and modulates  
621 presynaptic function and plasticity (de Juan-Sanz et al., 2017), roles that seem certain to  
622 contribute to a variety of neurological diseases.

623

## 624 **ACKNOWLEDGEMENTS**

625 We acknowledge the Bloomington Drosophila Stock Center and the Iowa Developmental  
626 Studies Hybridoma Bank for genetic and antibody reagents. We also thank Christopher Buser at  
627 Droseran LLC (Pasadena, CA) for technical assistance with electron microscopy. This work was  
628 supported in part by a USC Provost Fellowship to KK and by an NIH grant to DKD (NS019546),  
629 as well as funding from the Alfred P. Sloan, Ellison Medical, Mallinckrodt, Klingenstein-Simons,  
630 and Whitehall Foundations to DKD.

631

## 632 **AUTHOR CONTRIBUTIONS**

633 KK and DKD designed the research and KK, DK, DS, and XL performed experiments. KK, DK,  
634 DS, and XL analyzed data. KK and DKD wrote the manuscript.

635

636 The authors declare no competing financial interests.

637

## 638 **REFERENCES**

- 639 Aberle H, Haghighi AP, Fetter RD, McCabe BD, Magalhaes TR, Goodman CS (2002) wishful  
640 thinking encodes a BMP type II receptor that regulates synaptic growth in Drosophila.  
641 Neuron 33:545-558.  
642  
643 Aridor M, Fish KN (2009) Selective targeting of ER exit sites supports axon development. Traffic  
644 10:1669-1684.  
645  
646 Atwood HL, Govind CK, Wu CF (1993) Differential ultrastructure of synaptic terminals on ventral  
647 longitudinal abdominal muscles in Drosophila larvae. J Neurobiol 24:1008-1024.  
648

- 649 Bardo S, Cavazzini MG, Emptage N (2006) The role of the endoplasmic reticulum Ca<sup>2+</sup> store in  
650 the plasticity of central neurons. *Trends Pharmacol Sci* 27:78-84.  
651
- 652 Bassett AR, Liu JL (2014) CRISPR/Cas9 and genome editing in *Drosophila*. *J Genet Genomics*  
653 41:7-19.  
654
- 655 Beumer KJ, Carroll D (2014) Targeted genome engineering techniques in *Drosophila*. *Methods*  
656 68:29-37.  
657
- 658 Bischof J, Maeda RK, Hediger M, Karch F, Basler K (2007) An optimized transgenesis system  
659 for *Drosophila* using germ-line-specific phiC31 integrases. *Proc Natl Acad Sci U S A*  
660 104:3312-3317.  
661
- 662 Blackstone C, O'Kane CJ, Reid E (2011) Hereditary spastic paraplegias: membrane traffic and  
663 the motor pathway. *Nat Rev Neurosci* 12:31-42.  
664
- 665 Broadie K, Prokop A, Bellen HJ, O'Kane CJ, Schulze KL, Sweeney ST (1995) Syntaxin and  
666 synaptobrevin function downstream of vesicle docking in *Drosophila*. *Neuron* 15:663-  
667 673.  
668
- 669 Budnik V, Koh YH, Guan B, Hartmann B, Hough C, Woods D, Gorczyca M (1996) Regulation of  
670 synapse structure and function by the *Drosophila* tumor suppressor gene *dlg*. *Neuron*  
671 17:627-640.  
672
- 673 Carrasco S, Meyer T (2011) STIM proteins and the endoplasmic reticulum-plasma membrane  
674 junctions. *Annu Rev Biochem* 80:973-1000.  
675
- 676 Chang CL, Liou J (2016) Homeostatic regulation of the PI(4,5)P<sub>2</sub>-Ca<sup>2+</sup> signaling system at  
677 ER-PM junctions. *Biochim Biophys Acta* 1861:862-873.  
678
- 679 Chen CK, Bregere C, Paluch J, Lu JF, Dickman DK, Chang KT (2014) Activity-dependent  
680 facilitation of Synaptojanin and synaptic vesicle recycling by the Minibrain kinase. *Nat*  
681 *Commun* 5:4246.  
682
- 683 Chen X, Ma W, Zhang S, Paluch J, Guo W, Dickman DK (2017) The BLOC-1 Subunit Pallidin  
684 Facilitates Activity-Dependent Synaptic Vesicle Recycling. *eNeuro* 4.  
685
- 686 Choi BJ, Imlach WL, Jiao W, Wolfram V, Wu Y, Grbic M, Cela C, Baines RA, Nitabach MN,  
687 McCabe BD (2014) Miniature neurotransmission regulates *Drosophila* synaptic structural  
688 maturation. *Neuron* 82:618-634.  
689
- 690 Daniels RW, Collins CA, Gelfand MV, Dant J, Brooks ES, Krantz DE, DiAntonio A (2004)  
691 Increased expression of the *Drosophila* vesicular glutamate transporter leads to excess  
692 glutamate release and a compensatory decrease in quantal content. *J Neurosci*  
693 24:10466-10474.  
694
- 695 Davis GW, Muller M (2015) Homeostatic control of presynaptic neurotransmitter release. *Annu*  
696 *Rev Physiol* 77:251-270.  
697
- 698 De Camilli P, Emr SD, McPherson PS, Novick P (1996) Phosphoinositides as regulators in  
699 membrane traffic. *Science* 271:1533-1539.

700  
701 de Juan-Sanz J, Holt GT, Schreiter ER, de Juan F, Kim DS, Ryan TA (2017) Axonal  
702 Endoplasmic Reticulum Ca<sup>2+</sup> Content Controls Release Probability in CNS Nerve  
703 Terminals. *Neuron* 93:867-881 e866.  
704  
705 Di Paolo G, De Camilli P (2006) Phosphoinositides in cell regulation and membrane dynamics.  
706 *Nature* 443:651-657.  
707  
708 Di Paolo G, Moskowitz HS, Gipson K, Wenk MR, Voronov S, Obayashi M, Flavell R,  
709 Fitzsimonds RM, Ryan TA, De Camilli P (2004) Impaired PtdIns(4,5)P<sub>2</sub> synthesis in  
710 nerve terminals produces defects in synaptic vesicle trafficking. *Nature* 431:415-422.  
711  
712 Dickman DK, Davis GW (2009) The schizophrenia susceptibility gene dysbindin controls  
713 synaptic homeostasis. *Science* 326:1127-1130.  
714  
715 Dickman DK, Horne JA, Meinertzhagen IA, Schwarz TL (2005) A slowed classical pathway  
716 rather than kiss-and-run mediates endocytosis at synapses lacking synaptojanin and  
717 endophilin. *Cell* 123:521-533.  
718  
719 Dickman DK, Lu Z, Meinertzhagen IA, Schwarz TL (2006) Altered synaptic development and  
720 active zone spacing in endocytosis mutants. *Curr Biol* 16:591-598.  
721  
722 Dickson EJ, Jensen JB, Vivas O, Kruse M, Traynor-Kaplan AE, Hille B (2016) Dynamic  
723 formation of ER-PM junctions presents a lipid phosphatase to regulate  
724 phosphoinositides. *J Cell Biol* 213:33-48.  
725  
726 Dong B, Kakihara K, Otani T, Wada H, Hayashi S (2013) Rab9 and retromer regulate retrograde  
727 trafficking of luminal protein required for epithelial tube length control. *Nat Commun*  
728 4:1358.  
729  
730 Eden ER (2016) The formation and function of ER-endosome membrane contact sites. *Biochim*  
731 *Biophys Acta* 1861:874-879.  
732  
733 Fasana E, Fossati M, Ruggiano A, Brambillasca S, Hoogenraad CC, Navone F, Francolini M,  
734 Borgese N (2010) A VAPB mutant linked to amyotrophic lateral sclerosis generates a  
735 novel form of organized smooth endoplasmic reticulum. *FASEB J* 24:1419-1430.  
736  
737 Frank CA (2014) Homeostatic plasticity at the *Drosophila* neuromuscular junction.  
738 *Neuropharmacology* 78:63-74.  
739  
740 Frank CA, Kennedy MJ, Goold CP, Marek KW, Davis GW (2006) Mechanisms underlying the  
741 rapid induction and sustained expression of synaptic homeostasis. *Neuron* 52:663-677.  
742  
743 Giordano F, Saheki Y, Idevall-Hagren O, Colombo SF, Pirruccello M, Milosevic I, Gracheva EO,  
744 Bagriantsev SN, Borgese N, De Camilli P (2013) PI(4,5)P<sub>2</sub>-dependent and Ca<sup>2+</sup>-  
745 regulated ER-PM interactions mediated by the extended synaptotagmins. *Cell* 153:1494-  
746 1509.  
747  
748 Gratz SJ, Wildonger J, Harrison MM, O'Connor-Giles KM (2013a) CRISPR/Cas9-mediated  
749 genome engineering and the promise of designer flies on demand. *Fly (Austin)* 7:249-  
750 255.

751  
752 Gratz SJ, Cummings AM, Nguyen JN, Hamm DC, Donohue LK, Harrison MM, Wildonger J,  
753 O'Connor-Giles KM (2013b) Genome engineering of *Drosophila* with the CRISPR RNA-  
754 guided Cas9 nuclease. *Genetics* 194:1029-1035.  
755  
756 Hammond GR, Machner MP, Balla T (2014) A novel probe for phosphatidylinositol 4-phosphate  
757 reveals multiple pools beyond the Golgi. *J Cell Biol* 205:113-126.  
758  
759 Han C, Jan LY, Jan YN (2011) Enhancer-driven membrane markers for analysis of  
760 nonautonomous mechanisms reveal neuron-glia interactions in *Drosophila*. *Proc Natl*  
761 *Acad Sci U S A* 108:9673-9678.  
762  
763 Haucke V, Neher E, Sigrist SJ (2011) Protein scaffolds in the coupling of synaptic exocytosis  
764 and endocytosis. *Nat Rev Neurosci* 12:127-138.  
765  
766 Herdman C, Moss T (2016) Extended-Synaptotagmins (E-Syts); the extended story. *Pharmacol*  
767 *Res* 107:48-56.  
768  
769 Idevall-Hagren O, Lu A, Xie B, De Camilli P (2015) Triggered Ca<sup>2+</sup> influx is required for  
770 extended synaptotagmin 1-induced ER-plasma membrane tethering. *EMBO J* 34:2291-  
771 2305.  
772  
773 Jean S, Tremblay MG, Herdman C, Guillou F, Moss T (2012) The endocytic adapter E-Syt2  
774 recruits the p21 GTPase activated kinase PAK1 to mediate actin dynamics and FGF  
775 signalling. *Biol Open* 1:731-738.  
776  
777 Jean S, Mikryukov A, Tremblay MG, Baril J, Guillou F, Bellenfant S, Moss T (2010) Extended-  
778 synaptotagmin-2 mediates FGF receptor endocytosis and ERK activation in vivo. *Dev*  
779 *Cell* 19:426-439.  
780  
781 Khuong TM, Habets RL, Slabbaert JR, Verstreken P (2010) WASP is activated by  
782 phosphatidylinositol-4,5-bisphosphate to restrict synapse growth in a pathway parallel to  
783 bone morphogenetic protein signaling. *Proc Natl Acad Sci U S A* 107:17379-17384.  
784  
785 Koh TW, Verstreken P, Bellen HJ (2004) Dap160/intersectin acts as a stabilizing scaffold  
786 required for synaptic development and vesicle endocytosis. *Neuron* 43:193-205.  
787  
788 Kwon SK, Hirabayashi Y, Polleux F (2016) Organelle-Specific Sensors for Monitoring Ca<sup>2+</sup>  
789 Dynamics in Neurons. *Front Synaptic Neurosci* 8:29.  
790  
791 Lauwers E, Goodchild R, Verstreken P (2016) Membrane Lipids in Presynaptic Function and  
792 Disease. *Neuron* 90:11-25.  
793  
794 Lawe DC, Patki V, Heller-Harrison R, Lambright D, Corvera S (2000) The FYVE domain of early  
795 endosome antigen 1 is required for both phosphatidylinositol 3-phosphate and Rab5  
796 binding. Critical role of this dual interaction for endosomal localization. *J Biol Chem*  
797 275:3699-3705.  
798  
799 Lemmon MA (2003) Phosphoinositide recognition domains. *Traffic* 4:201-213.  
800

801 Mackler JM, Drummond JA, Loewen CA, Robinson IM, Reist NE (2002) The C(2)B Ca(2+)-  
802 binding motif of synaptotagmin is required for synaptic transmission in vivo. *Nature*  
803 418:340-344.  
804  
805 Manford AG, Stefan CJ, Yuan HL, Macgurn JA, Emr SD (2012) ER-to-plasma membrane  
806 tethering proteins regulate cell signaling and ER morphology. *Dev Cell* 23:1129-1140.  
807  
808 Marrus SB, Portman SL, Allen MJ, Moffat KG, DiAntonio A (2004) Differential localization of  
809 glutamate receptor subunits at the *Drosophila* neuromuscular junction. *J Neurosci*  
810 24:1406-1415.  
811  
812 Martin AR (1955) A further study of the statistical composition on the end-plate potential. *J*  
813 *Physiol* 130:114-122.  
814  
815 Meldolesi J (2001) Rapidly exchanging Ca<sup>2+</sup> stores in neurons: molecular, structural and  
816 functional properties. *Prog Neurobiol* 65:309-338.  
817  
818 Min SW, Chang WP, Sudhof TC (2007) E-Syts, a family of membranous Ca<sup>2+</sup>-sensor proteins  
819 with multiple C2 domains. *Proc Natl Acad Sci U S A* 104:3823-3828.  
820  
821 Montenegro G et al. (2012) Mutations in the ER-shaping protein reticulon 2 cause the axon-  
822 degenerative disorder hereditary spastic paraplegia type 12. *J Clin Invest* 122:538-544.  
823  
824 Muller M, Davis GW (2012) Transsynaptic control of presynaptic Ca(2)(+) influx achieves  
825 homeostatic potentiation of neurotransmitter release. *Curr Biol* 22:1102-1108.  
826  
827  
828 Muller M, Genc O, Davis GW (2015) RIM-binding protein links synaptic homeostasis to the  
829 stabilization and replenishment of high release probability vesicles. *Neuron* 85:1056-  
830 1069.  
831  
832 Muller M, Pym EC, Tong A, Davis GW (2011) Rab3-GAP controls the progression of synaptic  
833 homeostasis at a late stage of vesicle release. *Neuron* 69:749-762.  
834  
835 Muller M, Liu KS, Sigrist SJ, Davis GW (2012) RIM controls homeostatic plasticity through  
836 modulation of the readily-releasable vesicle pool. *J Neurosci* 32:16574-16585.  
837  
838 Nagarkar-Jaiswal S, Lee PT, Campbell ME, Chen K, Anguiano-Zarate S, Gutierrez MC, Busby  
839 T, Lin WW, He Y, Schulze KL, Booth BW, Evans-Holm M, Venken KJ, Levis RW,  
840 Spradling AC, Hoskins RA, Bellen HJ (2015) A library of MiMICs allows tagging of genes  
841 and reversible, spatial and temporal knockdown of proteins in *Drosophila*. *Elife* 4.  
842  
843 Nandi N, Tyra LK, Stenesen D, Kramer H (2014) Acinus integrates AKT1 and subapoptotic  
844 caspase activities to regulate basal autophagy. *J Cell Biol* 207:253-268.  
845  
846 Nemoto Y, Kearns BG, Wenk MR, Chen H, Mori K, Alb JG, Jr., De Camilli P, Bankaitis VA  
847 (2000) Functional characterization of a mammalian Sac1 and mutants exhibiting  
848 substrate-specific defects in phosphoinositide phosphatase activity. *J Biol Chem*  
849 275:34293-34305.  
850

- 851 Noreau A, Dion PA, Rouleau GA (2014) Molecular aspects of hereditary spastic paraplegia. *Exp*  
852 *Cell Res* 325:18-26.  
853
- 854 O'Connor-Giles KM, Ho LL, Ganetzky B (2008) Nervous wreck interacts with thickveins and the  
855 endocytic machinery to attenuate retrograde BMP signaling during synaptic growth.  
856 *Neuron* 58:507-518.  
857
- 858 O'Sullivan NC, Jahn TR, Reid E, O'Kane CJ (2012) Reticulon-like-1, the *Drosophila* orthologue  
859 of the hereditary spastic paraplegia gene reticulon 2, is required for organization of  
860 endoplasmic reticulum and of distal motor axons. *Hum Mol Genet* 21:3356-3365.  
861
- 862 Petkovic M, Jemaïel A, Daste F, Specht CG, Izeddin I, Vorkel D, Verbavatz JM, Darzacq X,  
863 Triller A, Pfenninger KH, Taresté D, Jackson CL, Galli T (2014) The SNARE Sec22b has  
864 a non-fusogenic function in plasma membrane expansion. *Nat Cell Biol* 16:434-444.  
865
- 866 Pfenninger KH (2009) Plasma membrane expansion: a neuron's Herculean task. *Nat Rev*  
867 *Neurosci* 10:251-261.  
868
- 869 Phillips MJ, Voeltz GK (2016) Structure and function of ER membrane contact sites with other  
870 organelles. *Nat Rev Mol Cell Biol* 17:69-82.  
871
- 872 Raiborg C, Wenzel EM, Pedersen NM, Olsvik H, Schink KO, Schultz SW, Vietri M, Nisi V, Bucci  
873 C, Brech A, Johansen T, Stenmark H (2015) Repeated ER-endosome contacts promote  
874 endosome translocation and neurite outgrowth. *Nature* 520:234-238.  
875
- 876 Ramirez OA, Couve A (2011) The endoplasmic reticulum and protein trafficking in dendrites and  
877 axons. *Trends Cell Biol* 21:219-227.  
878
- 879 Renvoise B, Blackstone C (2010) Emerging themes of ER organization in the development and  
880 maintenance of axons. *Curr Opin Neurobiol* 20:531-537.  
881
- 882 Rodal AA, Blunk AD, Akbergenova Y, Jorquera RA, Buhl LK, Littleton JT (2011) A presynaptic  
883 endosomal trafficking pathway controls synaptic growth signaling. *J Cell Biol* 193:201-  
884 217.  
885
- 886 Rowland AA, Chitwood PJ, Phillips MJ, Voeltz GK (2014) ER contact sites define the position  
887 and timing of endosome fission. *Cell* 159:1027-1041.  
888
- 889 Saheki Y, De Camilli P (2017) The Extended-Synaptotagmins. *Biochim Biophys Acta*.  
890
- 891 Saheki Y, Bian X, Schauder CM, Sawaki Y, Surma MA, Klose C, Pincet F, Reinisch KM, De  
892 Camilli P (2016) Control of plasma membrane lipid homeostasis by the extended  
893 synaptotagmins. *Nat Cell Biol* 18:504-515.  
894
- 895 Sclip A, Bacaj T, Giam LR, Sudhof TC (2016) Extended Synaptotagmin (ESyt) Triple Knock-Out  
896 Mice Are Viable and Fertile without Obvious Endoplasmic Reticulum Dysfunction. *PLoS*  
897 *One* 11:e0158295.  
898
- 899 Sebo ZL, Lee HB, Peng Y, Guo Y (2014) A simplified and efficient germline-specific  
900 CRISPR/Cas9 system for *Drosophila* genomic engineering. *Fly (Austin)* 8:52-57.  
901

- 902 Simonsen A, Lippe R, Christoforidis S, Gaullier JM, Brech A, Callaghan J, Toh BH, Murphy C,  
903 Zerial M, Stenmark H (1998) EEA1 links PI(3)K function to Rab5 regulation of endosome  
904 fusion. *Nature* 394:494-498.  
905
- 906 Slabbaert JR, Khuong TM, Verstreken P (2012) Phosphoinositides at the neuromuscular  
907 junction of *Drosophila melanogaster*: a genetic approach. *Methods Cell Biol* 108:227-  
908 247.  
909
- 910 Spacek J, Harris KM (1997) Three-dimensional organization of smooth endoplasmic reticulum in  
911 hippocampal CA1 dendrites and dendritic spines of the immature and mature rat. *J*  
912 *Neurosci* 17:190-203.  
913
- 914 Stenmark H, Vitale G, Ullrich O, Zerial M (1995) Rabaptin-5 is a direct effector of the small  
915 GTPase Rab5 in endocytic membrane fusion. *Cell* 83:423-432.  
916
- 917 Stewart BA, Atwood HL, Renger JJ, Wang J, Wu CF (1994) Improved stability of *Drosophila*  
918 larval neuromuscular preparations in haemolymph-like physiological solutions. *J Comp*  
919 *Physiol A* 175:179-191.  
920
- 921 Stutzmann GE, Mattson MP (2011) Endoplasmic reticulum Ca(2+) handling in excitable cells in  
922 health and disease. *Pharmacol Rev* 63:700-727.  
923
- 924 Summerville JB, Faust JF, Fan E, Pendin D, Daga A, Formella J, Stern M, McNew JA (2016)  
925 The effects of ER morphology on synaptic structure and function in *Drosophila*  
926 *melanogaster*. *J Cell Sci* 129:1635-1648.  
927
- 928 Sweeney ST, Broadie K, Keane J, Niemann H, O'Kane CJ (1995) Targeted expression of  
929 tetanus toxin light chain in *Drosophila* specifically eliminates synaptic transmission and  
930 causes behavioral defects. *Neuron* 14:341-351.  
931
- 932 Terasaki M, Slater NT, Fein A, Schmidek A, Reese TS (1994) Continuous network of  
933 endoplasmic reticulum in cerebellar Purkinje neurons. *Proc Natl Acad Sci U S A*  
934 91:7510-7514.  
935
- 936 Tremblay MG, Moss T (2016) Loss of all 3 Extended Synaptotagmins does not affect normal  
937 mouse development, viability or fertility. *Cell Cycle* 15:2360-2366.  
938
- 939 Tremblay MG, Herdman C, Guillou F, Mishra PK, Baril J, Bellenfant S, Moss T (2015) Extended  
940 Synaptotagmin Interaction with the Fibroblast Growth Factor Receptor Depends on  
941 Receptor Conformation, Not Catalytic Activity. *J Biol Chem* 290:16142-16156.  
942
- 943 Tsukita S, Ishikawa H (1976) Three-dimensional distribution of smooth endoplasmic reticulum in  
944 myelinated axons. *J Electron Microsc (Tokyo)* 25:141-149.  
945
- 946 Venken KJ, Schulze KL, Haelterman NA, Pan H, He Y, Evans-Holm M, Carlson JW, Levis RW,  
947 Spradling AC, Hoskins RA, Bellen HJ (2011) MiMIC: a highly versatile transposon  
948 insertion resource for engineering *Drosophila melanogaster* genes. *Nat Methods* 8:737-  
949 743.  
950
- 951 Verkhatsky A (2005) Physiology and pathophysiology of the calcium store in the endoplasmic  
952 reticulum of neurons. *Physiol Rev* 85:201-279.

- 953  
954 Verstreken P, Ohyama T, Bellen HJ (2008) FM 1-43 labeling of synaptic vesicle pools at the  
955 *Drosophila* neuromuscular junction. *Methods Mol Biol* 440:349-369.  
956  
957 Verstreken P, Kjaerulf O, Lloyd TE, Atkinson R, Zhou Y, Meinertzhagen IA, Bellen HJ (2002)  
958 Endophilin mutations block clathrin-mediated endocytosis but not neurotransmitter  
959 release. *Cell* 109:101-112.  
960  
961 Verstreken P, Koh TW, Schulze KL, Zhai RG, Hiesinger PR, Zhou Y, Mehta SQ, Cao Y, Roos J,  
962 Bellen HJ (2003) Synaptojanin is recruited by endophilin to promote synaptic vesicle  
963 uncoating. *Neuron* 40:733-748.  
964  
965 Verstreken P, Ohyama T, Haueter C, Habets RL, Lin YQ, Swan LE, Ly CV, Venken KJ, De  
966 Camilli P, Bellen HJ (2009) Tweek, an evolutionarily conserved protein, is required for  
967 synaptic vesicle recycling. *Neuron* 63:203-215.  
968  
969 Wang X, Shaw WR, Tsang HT, Reid E, O'Kane CJ (2007) *Drosophila* spichthyn inhibits BMP  
970 signaling and regulates synaptic growth and axonal microtubules. *Nat Neurosci* 10:177-  
971 185.  
972  
973 Wenk MR, De Camilli P (2004) Protein-lipid interactions and phosphoinositide metabolism in  
974 membrane traffic: insights from vesicle recycling in nerve terminals. *Proc Natl Acad Sci*  
975 *U S A* 101:8262-8269.  
976  
977 Wenk MR, Lucast L, Di Paolo G, Romanelli AJ, Suchy SF, Nussbaum RL, Cline GW, Shulman  
978 GI, McMurray W, De Camilli P (2003) Phosphoinositide profiling in complex lipid  
979 mixtures using electrospray ionization mass spectrometry. *Nat Biotechnol* 21:813-817.  
980  
981 Wong CO, Chen K, Lin YQ, Chao Y, Duraine L, Lu Z, Yoon WH, Sullivan JM, Broadhead GT,  
982 Sumner CJ, Lloyd TE, Macleod GT, Bellen HJ, Venkatachalam K (2014) A TRPV  
983 channel in *Drosophila* motor neurons regulates presynaptic resting Ca<sup>2+</sup> levels, synapse  
984 growth, and synaptic transmission. *Neuron* 84:764-777.  
985  
986 Wucherpennig T, Wilsch-Brauninger M, Gonzalez-Gaitan M (2003) Role of *Drosophila* Rab5  
987 during endosomal trafficking at the synapse and evoked neurotransmitter release. *J Cell*  
988 *Biol* 161:609-624.  
989  
990 Yang YS, Harel NY, Strittmatter SM (2009) Reticulon-4A (Nogo-A) redistributes protein disulfide  
991 isomerase to protect mice from SOD1-dependent amyotrophic lateral sclerosis. *J*  
992 *Neurosci* 29:13850-13859.  
993  
994 Yu H, Liu Y, Gulbranson DR, Paine A, Rathore SS, Shen J (2016) Extended synaptotagmins  
995 are Ca<sup>2+</sup>-dependent lipid transfer proteins at membrane contact sites. *Proc Natl Acad*  
996 *Sci U S A* 113:4362-4367.  
997  
998 Yu Z, Ren M, Wang Z, Zhang B, Rong YS, Jiao R, Gao G (2013) Highly efficient genome  
999 modifications mediated by CRISPR/Cas9 in *Drosophila*. *Genetics* 195:289-291.  
1000  
1001 Zhang C, Wu B, Beglopoulos V, Wines-Samuelson M, Zhang D, Dragatsis I, Sudhof TC, Shen J  
1002 (2009) Presenilins are essential for regulating neurotransmitter release. *Nature* 460:632-  
1003 636.



1004

1005 **FIGURE LEGENDS**

1006 **Figure 1: Generation and analysis of null mutations in *Drosophila Esyt*.** (A) Schematic of  
1007 the *Drosophila Esyt* locus. The CRISPR induced early stop codon in *Esy<sup>t1</sup>* (red asterisk) and the  
1008 MiMIC transposon insertion site of *Esy<sup>t2</sup>* (red triangle) are shown. (B) Schematic of the mouse  
1009 *Esy<sup>t</sup>* protein structure aligned with the *Drosophila* homolog. The *Esy<sup>t</sup>* proteins contain a  
1010 hydrophobic stretch (HS), synaptotagmin-like-mitochondrial lipid-binding protein (SMP), followed  
1011 by C<sub>2</sub> domains (C<sub>2</sub>). The *Esy<sup>t</sup>* domain structure is highly conserved between *Drosophila* to mice.  
1012 *Esy<sup>t1</sup>* and *Esy<sup>t2</sup>* mutations truncate the open reading frame before the HS domain. Red line  
1013 indicates the antigen the antibody was raised against. The structure of *Esy<sup>t</sup>* transgenes are also  
1014 shown. Western blot analyses of *Esy<sup>t</sup>* in adult heads (C) and larval CNS (D) demonstrates the  
1015 nervous system expression of *Esy<sup>t</sup>* and confirms both *Esy<sup>t1</sup>* and *Esy<sup>t2</sup>* are protein nulls.  
1016 Neuronal overexpression of *Esy<sup>t</sup>* (*Esy<sup>t</sup>Flag-OE: w;OK6-Gal4/UAS-Esy<sup>t</sup>Flag* and *Esy<sup>t</sup>mCh-OE:*  
1017 *w;OK6-Gal4/UAS-Esy<sup>t</sup>mCh*) results in elevated levels and increased molecular mass observed  
1018 for the tagged transgene, as expected. Anti-Actin was used as loading control.

1019

1020 **Figure 2: The hydrophobic stretch is necessary to localize *Esy<sup>t</sup>* to axonal ER.** (A)  
1021 Representative images of third-instar larval NMJ with motor neuron expression of an mCherry-  
1022 tagged *Esy<sup>t</sup>* transgene (mCherry; magenta) and a GFP-tagged ER retention signal KDEL (GFP;  
1023 green; *w;OK6-Gal4/UAS-Esy<sup>t</sup>mCh;UAS-GFP-KDEL*), immunolabeled with the neuronal  
1024 membrane marker HRP (white/blue). *Esy<sup>t</sup>-mCherry* colocalizes with axonal ER labeled by GFP-  
1025 KDEL. (B) Deletion of the hydrophobic stretch from *Esy<sup>t</sup>-mCherry* (*w;OK6-Gal4/UAS-*  
1026 *Esy<sup>t</sup>AHS;UAS-GFP-KDEL*) results in a failure to localize to the ER, instead acquiring a cytosolic  
1027 distribution. (C) Representative NMJ images of a Flag-tagged *Esy<sup>t</sup>* transgene (*Esy<sup>t</sup>Flag: w;OK6-*  
1028 *Gal4/UAS-Esy<sup>t</sup>Flag*) expressed in motor neurons (anti-Flag; magenta) and labeled with HRP  
1029 (white/blue). *Esy<sup>t</sup>-Flag* traffics to the presynaptic terminals similarly to *Esy<sup>t</sup>-mCherry*. (D)

1030 Mutations in an *Esy<sup>tFlag</sup>* transgene that prevent Ca<sup>2+</sup> binding to C2 domains (*Esy<sup>tD-N</sup>*: *w;OK6-*  
1031 *Gal4/UAS-Esy<sup>tD-N</sup>*) no longer traffics to presynaptic terminals. **(E)** Axonal ER structures labeled  
1032 with *Esy<sup>tFlag</sup>* (anti-Flag; magenta) is shown relative to active zones (BRP; green) and synaptic  
1033 vesicle structures (vGlut; white/blue). **(F)** Axonal ER labeled by *Esy<sup>tFlag</sup>* is shown co-labeled  
1034 with a peri-active zone marker (FasII; green) and a neuronal membrane marker (HRP;  
1035 white/blue).

1036

1037 **Figure 3: PI(4,5)P<sub>2</sub> and PI(3)P phospholipid levels are unchanged at presynaptic terminals**  
1038 **in *Esy<sup>t</sup>* mutants and *Esy<sup>t</sup>*-OE. **(A)** Representative NMJ images of PI(4,5)P<sub>2</sub> labeled with PLCδ-  
1039 PH-GFP (GFP; green) and HRP (white/blue) in control (*w;OK6-Gal4/+;UAS-PLCδ-PH-GFP/+*),  
1040 *Esy<sup>t</sup>* mutants (*w;OK6-Gal4/+;Esy<sup>t1</sup>/Esy<sup>t2</sup>,UAS-PLCδ-PH-GFP*), and *Esy<sup>t</sup>*-OE (*w;OK6-*  
1041 *Gal4/UAS-Esy<sup>t<sup>mCh</sup></sup>;UAS-PLCδ1-PH-GFP/+*). **(B)** Quantification of mean GFP intensity levels of  
1042 the indicated genotypes. **(C)** Representative images of PI(3)P distribution at the NMJ labeled by  
1043 GFP-myc-2xFYVE in control (*w;OK6-Gal4/UAS-GFP-myc-2xFYVE*), *Esy<sup>t</sup>* mutants (*w;OK6-*  
1044 *Gal4/UAS-GFP-myc-2xFYVE;Esy<sup>t1</sup>/Esy<sup>t2</sup>*), and *Esy<sup>t</sup>*-OE (*w;OK6-Gal4/UAS-GFP-myc-*  
1045 *2xFYVE;UAS-Esy<sup>tFlag</sup>/+*). **(D)** Quantification of mean GFP intensity levels of the indicated  
1046 genotypes. Error bars indicate ±SEM. One-way analysis of variance (ANOVA) test was  
1047 performed, followed by a Tukey's multiple-comparison test. NS=not significant, p>0.05. Detailed  
1048 statistical information for represented data (mean values, SEM, n, p) is shown in Table 1.**

1049

1050 **Figure 4: Presynaptic overexpression of *Esy<sup>t</sup>* promotes synaptic growth. **(A)****

1051 Representative NMJ images of wild type (*w<sup>1118</sup>*), *Esy<sup>t</sup>* mutants (*Esy<sup>t1/2</sup>*: *w;Esy<sup>t1</sup>/Esy<sup>t2</sup>*), and *Esy<sup>t</sup>*-  
1052 OE (*Esy<sup>t<sup>mCh</sup></sup>*-OE: *w;OK6-Gal4/UAS-Esy<sup>t<sup>mCh</sup></sup>* and *Esy<sup>tFlag</sup>*-OE: *w;OK6-Gal4/UAS-Esy<sup>tFlag</sup>*)  
1053 immunostained for anti-BRP (green), anti-GluRIII (magenta), and anti-HRP (white; insert).  
1054 Bottom panels: BRP and GluRIII images at higher magnification. Quantification of bouton  
1055 number per NMJ **(B)**, neuronal membrane surface area **(C)**, total BRP puncta number per NMJ

1056 **(D)**, BRP density **(E)**, and BRP area **(F)** of the indicated genotypes. Note that *Esyt*-OE results in  
1057 increased bouton number and a corresponding increase in membrane and BRP number. Error  
1058 bars indicate  $\pm$ SEM. One-way ANOVA test was performed, followed by a Tukey's multiple-  
1059 comparison test. \*\* $p < 0.01$ ; \*\*\* $p < 0.001$ . Detailed statistical information for represented data (mean  
1060 values, SEM, n, p) is shown in Table 1.

1061

1062 **Figure 5: Synaptic transmission and vesicle depletion in *Esyt* mutants and *Esyt*-OE. (A)**

1063 Representative electrophysiological EPSP and mEPSP traces for wild type, *Esyt* mutants  
1064 (*Esyt*<sup>1/2</sup> and *Esyt*<sup>1/Df</sup>; *w*; *Esyt*<sup>1</sup>/*Esyt*<sup>Df</sup>) and *Esyt*-OE recorded in 0.4 mM extracellular Ca<sup>2+</sup>.

1065 Quantification of mEPSP amplitude **(B)**, EPSP amplitude **(C)**, and quantal content **(D)** of the  
1066 indicated genotypes. *Esyt* mutants exhibit no significant differences in synaptic transmission  
1067 compared to wild type, while *Esyt*-OE results in a moderate but significant increase in EPSP  
1068 amplitude. **(E)** Depletion and recovery of the functional vesicle pool in the indicated genotypes.  
1069 NMJs were stimulated at 10 Hz for 10 min in 10 mM extracellular Ca<sup>2+</sup>, then allowed to recover  
1070 for 10 mins while monitoring this recovery with stimulation at 0.2 Hz. EPSP amplitudes were  
1071 averaged, normalized to pre-stimulus amplitudes, and plotted as a function of time. **(F)**  
1072 Quantification of total quanta released during the 10 mins of 10 Hz stimulation for the indicated  
1073 genotypes. Error bars indicate  $\pm$ SEM. One-way ANOVA test was performed, followed by a  
1074 Tukey's multiple-comparison test. \* $p \leq 0.05$ ; \*\*\* $p < 0.001$ . Detailed statistical information for  
1075 represented data (mean values, SEM, n, p) is shown in Table 1.

1076

1077 **Figure 6: Synaptic vesicle density and endocytic pools are unchanged in *Esyt* mutants**

1078 **and *Esyt*-OE. (A)** Representative electron micrograph images of NMJs for wild type, *Esyt*  
1079 mutants, and *Esyt*<sup>Flag</sup>-OE. Quantification of synaptic vesicle density **(B)**, synaptic vesicles within  
1080 300 nm of the active zone **(C)**, T bar length **(D)**, and active zone length **(E)** in the indicated  
1081 genotypes. No significant differences were observed between genotypes. **(F)** Representative

1082 images of FM1-43 dye loading of the indicated genotypes. **(G)** Quantification of mean intensity  
1083 of the FM1-43 signal in the indicated genotypes. Error bars indicate  $\pm$ SEM. One-way ANOVA  
1084 test was performed, followed by a Tukey's multiple-comparison test. NS=not significant,  $p>0.05$ .  
1085 Detailed statistical information for represented data (mean values, SEM, n, p) is shown in Table  
1086 1.

1087

1088 **Figure 7: *Esy1* is required for basal neurotransmission and short-term synaptic plasticity**  
1089 **at elevated extracellular  $Ca^{2+}$ .** **(A)** Quantal content plotted as a function of extracellular  $Ca^{2+}$   
1090 concentration on logarithmic scales for wild type, *Esy1* mutants (*Esy1<sup>1/2</sup>*), and *Esy1<sup>Flag</sup>*-OE. No  
1091 significant difference was observed in the slope of the best fit lines. **(B)** Representative EPSC  
1092 traces following four pulses of 60 Hz stimulation in wild type (black), *Esy1* mutants (*Esy1<sup>1/2</sup>*, red),  
1093 *Esy1* neuronal rescue (*w;OK6-Gal4/UAS-Esy1<sup>Flag</sup>; Esy1<sup>1</sup>/Esy1<sup>2</sup>*), and *Esy1<sup>Flag</sup>*-OE (blue) in 3 mM  
1094 extracellular  $Ca^{2+}$ . **(C)** Quantification of average EPSC amplitude in the indicated genotypes. **(D)**  
1095 Quantification of average EPSC ratio (4<sup>th</sup> EPSC/1<sup>st</sup> EPSC) for the indicated genotypes. *Esy1*  
1096 mutants show reduced neurotransmission and short-term synaptic plasticity at high extracellular  
1097  $Ca^{2+}$ . Error bars indicate  $\pm$ SEM. One-way ANOVA test was performed, followed by a Tukey's  
1098 multiple-comparison test. \* $p\leq 0.05$ ; \*\* $p\leq 0.01$ . Detailed statistical information for represented data  
1099 (mean values, SEM, n, p) is shown in Table 1.

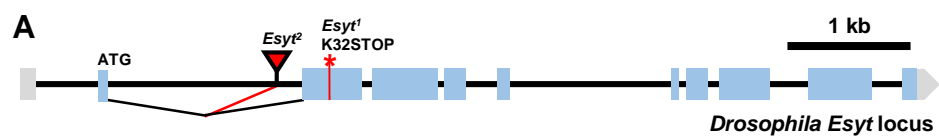
1100

1101 **Figure 8: *Esy1* is dispensable for presynaptic homeostatic plasticity.** **(A)** Representative  
1102 electrophysiological EPSP and mEPSP traces for wild type, *Esy1* mutants (*Esy1<sup>1/2</sup>*), and *Esy1<sup>Flag</sup>*-  
1103 OE before (baseline) and following PhTx application. Note that while mEPSP amplitudes are  
1104 reduced following PhTx application, EPSP amplitudes recover to baseline levels because of a  
1105 homeostatic increase in presynaptic release (quantal content). **(B)** Quantification of mEPSP and  
1106 quantal content values after PhTx application normalized to baseline values. No significant  
1107 differences were observed. Error bars indicate  $\pm$ SEM. One-way ANOVA test was performed,

1108 followed by a Tukey's multiple-comparison test. Detailed statistical information for represented  
1109 data (mean values, SEM, n, p) is shown in Table 1.

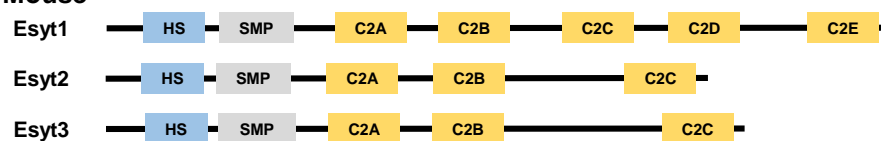
1110

1111 **Table 1: Absolute and additional values for normalized and presented data.** The figure and  
1112 panel, genotype, and conditions used are noted (external  $\text{Ca}^{2+}$  concentration as well as whether  
1113 PhTx was applied or not). Average values with standard error values noted in parentheses are  
1114 shown for all morphology data such as neuronal membrane surface area, bouton number, as  
1115 well as intensity values for all represented synaptic proteins and postsynaptic glutamate  
1116 receptors are shown. For electrophysiological experiments, all passive membrane properties  
1117 (input resistance, resting membrane potential), and mEPSP, EPSP, QC, number of data  
1118 samples (n) and p-values from the statistical test are shown.

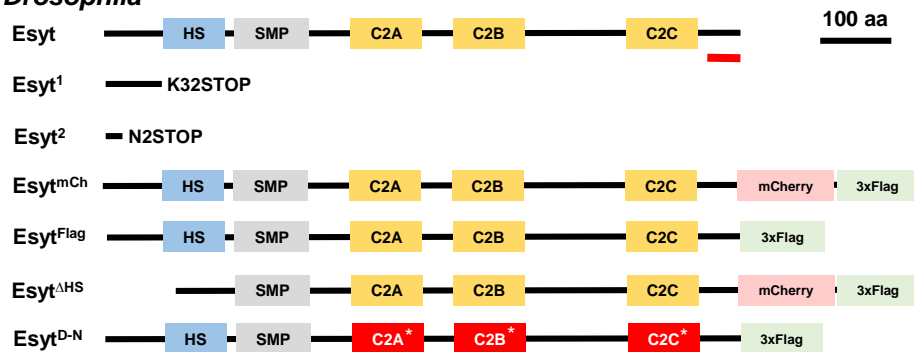


**B**

**Mouse**

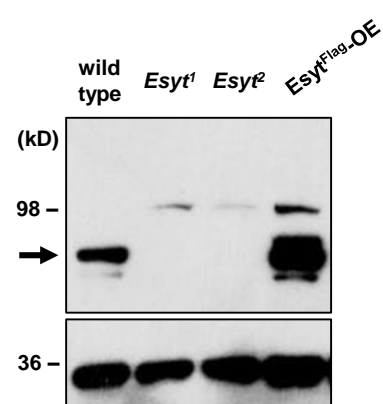


**Drosophila**



**C**

Adult Head



**D**

Larval CNS

